Vascular design for reducing hot spots and stresses

L. A. O. Rocha, S. Lorente, and A. Bejan

Citation: Journal of Applied Physics **115**, 174904 (2014); doi: 10.1063/1.4874220
View online: http://dx.doi.org/10.1063/1.4874220
View Table of Contents: http://scitation.aip.org/content/aip/journal/jap/115/17?ver=pdfcov
Published by the AIP Publishing

Vascular design for reducing hot spots and stresses

L. A. O. Rocha,[1] S. Lorente,[2] and A. Bejan[3,a)]
[1]*Departamento de Engenharia Mecânica, Universidade Federal do Rio Grande do Sul, Porto Alegre, RS, Brazil*
[2]*Departement de Genie Civil, Institut National des Sciences Appliquées, 135 Avenue de Rangueil, 31077 Toulouse, France*
[3]*Department of Mechanical Engineering and Materials Science, Duke University, Box 90300, Durham, North Carolina 27708-0300, USA*

(Received 6 March 2014; accepted 19 April 2014; published online 5 May 2014)

This paper is a proposal to embed tree-shaped vasculatures in a wall designed such that the wall withstands without excessive hot spots and peak stresses the intense heating and pressure that impinge on it. The vasculature is a quilt of square-shaped panels, each panel having a tree vasculature that connects the center with the perimeter. The vascular designs for volumetric cooling can be complemented by the shaping and distributing of channels for maximum strength and thermal performance at the same time. Numerical simulations of heat flow and thermal stresses in three directions show that it is possible to determine the optimal geometric features of configurations with radial channels and trees with radial and one level of bifurcations. The global performance is evaluated in terms of the overall thermal resistance and peak von Mises stresses. The dendritic design is superior under the studied thermal condition. © *2014 AIP Publishing LLC*. [http://dx.doi.org/10.1063/1.4874220]

I. VASCULAR DESIGN

Dendritic structures for high-density volumetric cooling were proposed when the constructal law was formulated.[1,2] The first designs were for heat conduction, with tree-shaped paths made out of high-conductivity inserts. The initial work on tree-shaped flow architectures was based on three approaches. It started in 1996 with an analytical shortcut[1] based on several simplifying assumptions: 90° angles between stem and tributaries, in a construction sequence in which smaller optimized constructs are retained, constant-thickness branches, and so on. Months later, we solved the same problem numerically[3] by abandoning most of the simplifying assumptions (e.g., the compounding construction sequence) used in the first papers. In 1998, we reconsidered the problem in an area-to-point flow domain with randomly moving low-resistivity blocks embedded in a high-resistivity background[4,5] with Darcy flow (permeability instead of conductivity and resistivity). Grains of high resistivity were identified and replaced with grains of low resistivity in such a way that the global resistance of the area-to-point flow decreased in every frame of the evolutionary design. Along the way, we found better performance and trees that look more "natural" as we progress in time, that is, as we endowed the flow structure with more freedom to morph.

The growth of the constructal-law field is reviewed regularly.[6–12] A distinct trend in constructal design is the development of vascular flow architectures, which fill bodies (structural members) and endow them with volumetrically distributed functions such as self healing[13,14] and self cooling.[15] This work is driven by applications to smart materials, smart structures, the design of future aircraft,[16] and the cooling of progressively more compact electronics.

On the fundamental side, the key question is why should a "vascular" flow architecture emerge in the animal, and in the engineered smart body? "Vascular" means that the stream bathes the entire volume almost uniformly, by flowing as two trees matched canopy to canopy.[17] First, the stream enters the volume by distributing its flow like a river delta. Second, the stream reconstitutes itself and flows out of the volume like a river basin. Kim *et al.*[18] showed that tree-tree architectures recommend themselves for all the volumes bathed by single streams in laminar flow, and that in larger volumes, each tree must have more levels of branching or coalescence. Cetkin *et al.*[19] demonstrated the same trend for trees with turbulent flow.

The vascular design literature is expanding rapidly, from architectures for self healing[20,21] to trees matched canopy to canopy in vascular bodies.[22–31] Thermal characteristics and the heat transfer performance of vascular designs are documented in Refs. 32–39. Vascular porous structures were designed for electrokinetic mass transfer[40] and for heat transfer in biological tissues.[41–44] Vascular designs for cooling a plate heated by a randomly moving energy beam were developed by Cetkin *et al.*[45]

Design occurs in nature not only in fluid flow systems such as river basins and human lungs but also in solid structures such as animal skeletons,[46] vegetation,[47] and bodies of vehicles.[48] Solid structures were brought under the Constructal law by the view that they are bodies shaped for the flow of stresses.[47,49] When stresses flow from one end to the other of a structural member without obstacles (strangulations, stress concentrations), the member carries the imposed load with minimum material. The easiest flow of stresses means the lightest and strongest member, and the

a)Author to whom correspondence should be addressed. Electronic mail: dalford@duke.edu.

most efficient animal or vehicle that uses that member as support structure. At bottom, the constructal design of the flow of stresses in solids is a manifestation of the grand constructal design of the flow of mass on the globe.

The flow of stresses as a morphing flow system was proposed[47] in order to predict the entire architecture of vegetation, from roots to trunks, canopies and the floor of the forest. Since then, the flow of stresses has become an integral part of constructal design.[49] Plates can be shaped (tapered) so that stresses flow through them in "boundary layer" fashion.[50] Bars and linkages in compression and buckling can be shaped and sized so that they carry their loads with minimal material. The vascular designs for volumetric cooling can be complemented by the shaping and distributing of channels for maximum strength and thermal performance at the same time.[51–53]

In this paper, we explore the design of a vascular body with two functions at the same time: volumetric cooling and mechanical strength (Fig. 1). The objective is to identify the architectural features that limit the formation of hot spots and peak stresses in the body volume.

II. NUMERICAL MODEL

Consider first the three-dimensional structure shown in Fig. 2. The body is a square slab $2L \times 2L$ with the thickness t. It is insulated except on the bottom surface where it receives the uniform heat flux q''. It is cooled by fluid that flows through ducts of square cross-section ($D_0 \times D_0$), which are embedded in the slab. The ducts are dug into the top surface of the slab. They continue with 90° turns [see the position (0, y_1, t)] and lead to the bottom surface where they bifurcate on the way to the two outlets located in the corners of the bottom surface. When solving the conduction equation applied to the solid body, we are using the assumption that the flow is fast enough and the channels short enough, therefore, we can assume that the flow has a constant heat transfer coefficient h and a constant temperature T_∞, which are used as thermal boundary conditions on the surfaces bathed by the fluid.

There are two objectives: to minimize the hot-spot temperatures regardless of their location and to find

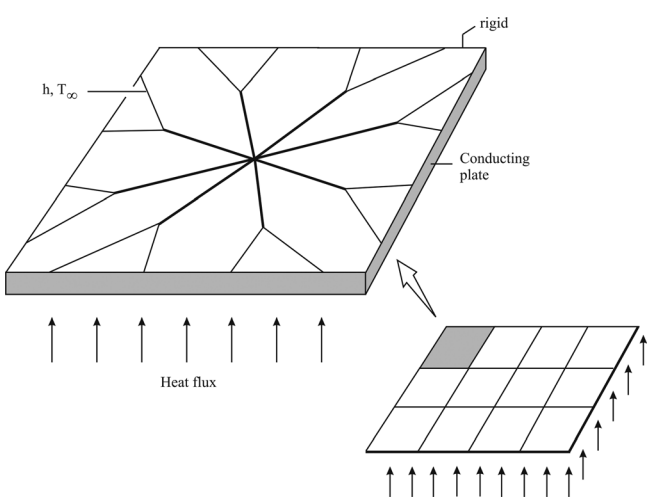

FIG. 1. Constructal "fire wall" concept with embedded dendritic coolant architecture.

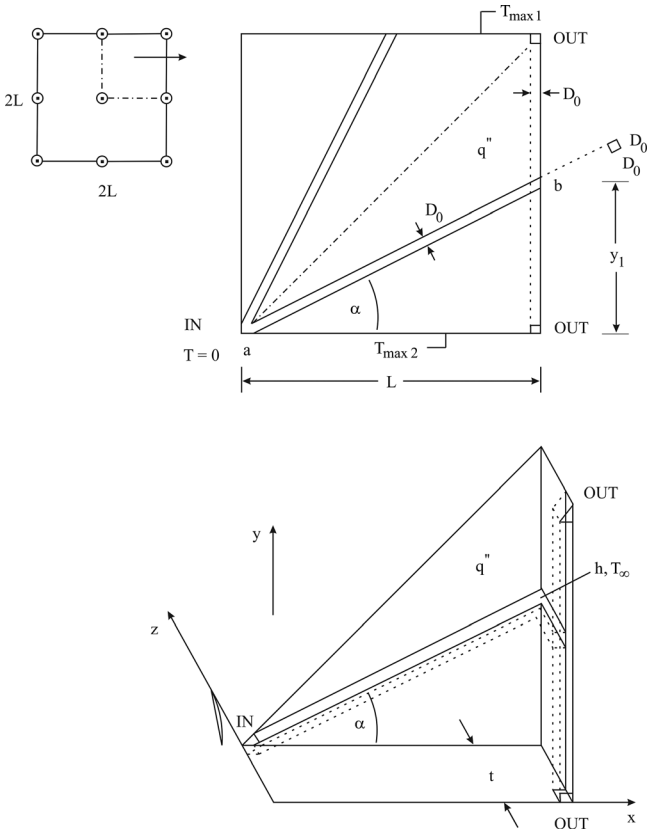

FIG. 2. Design with radial channels for cooling a square slab heated uniformly on its bottom side.

configurations with progressively smaller von Mises stress σ_{vM}, such the loss in mechanical strength due to the presence of channels is minimized. Because of symmetry, we consider only one-eighth of the body. There are two constraints to consider. One is the total volume of one-eighth of the slab

$$V_t = \frac{1}{2}L^2 t. \tag{1}$$

The other constraint is the volume occupied by the ducts

$$V_p = \left(\frac{L}{\cos\alpha} + t + L + \frac{\sin(\pi/4+\alpha)\sin(\pi/2-\alpha)}{2\sin(\pi/4)}D_0 - \frac{5}{2}D_0\right)D_0^2, \tag{2}$$

where the angle α is defined in Fig. 2. The V_p and V_t constraints can be combined to define the fixed volume fraction occupied by ducts

$$\phi = \frac{V_p}{V_t}. \tag{3}$$

The structure of Fig. 2 was morphed numerically by simulating the three-dimensional temperature field and the stresses in a large number of configurations. This was achieved by varying the coordinates of point b (0, y_1, t), or the angle α, and calculating the maximum temperature, T_{max}, and the maximum von Mises stress, $\sigma_{vM,max}$. The search was

for configurations with smaller T_{max} and smaller $\sigma_{vM,max}$. The governing equations were nondimensionalized by defining the dimensionless variables

$$\left(\tilde{u}, \tilde{v}, \tilde{w}, \tilde{x}, \tilde{y}, \tilde{z}, \tilde{D}_0, \tilde{t}\right) = (u, v, w, x, y, z, D_0, t)/L, \quad (4)$$

$$\left(\tilde{\sigma}, \tilde{\tau}, \tilde{E}, \tilde{P}_{mech}\right) = (\sigma, \tau, E, P_{mech})/P_{mech}, \quad (5)$$

where u, v, and w are the displacements in the x, y, and z directions, respectively, and where σ and τ are the normal and shear stresses. Furthermore, E is Young's modulus and P_{mech} is the pressure applied uniformly from the upper surface. The dimensionless three-dimensional equation for steady state conduction in the solid body is

$$\frac{\partial^2\theta}{\partial\tilde{x}^2} + \frac{\partial^2\theta}{\partial\tilde{y}^2} + \frac{\partial^2\theta}{\partial\tilde{z}^2} = 0, \quad (6)$$

with the dimensionless temperature difference defined as

$$\theta = \frac{T - T_\infty}{q''L/k}, \quad (7)$$

where T, T_∞, q'', A, k_s, and L are the solid temperature, fluid temperature, heat flux in the bottom surface, area of one-fourth of the slab ($A = L^2$), solid thermal conductivity, and length of one-fourth of the slab, respectively. The coordinates x, y, and z are indicated in Fig. 2. The boundary conditions are as follows:

On the bottom surface

$$\frac{\partial\theta}{\partial\tilde{z}} = -1. \quad (8)$$

On the surfaces bathed by the fluid

$$\frac{\partial\theta}{\partial\tilde{n}} = -\lambda\theta, \quad (9)$$

where

$$\lambda = \frac{hL}{k_s}, \quad (10)$$

and on all the other surfaces,

$$\frac{\partial\theta}{\partial\tilde{n}} = \theta. \quad (11)$$

In the thermally fully developed Hagen-Poiseuille flow $\lambda_{lam} \cong 4(L/D_h)(k_f/k_s)$ while for a turbulent flow $\lambda_{turb} \cong 0.023 Re_D^{0.8} Pr^{0.4}(k_f/k_s)$.[54,55] For example, for $k_{water} = 0.6$ W/mK and $k_{steel} = 15$ W/mK, $\lambda_{lam} \approx 50$. On the other hand, if $(k_f/k_s) = 0.9$, $\lambda_{turb} \approx 10$ when $Re_D \approx 2700$. In sum, the parameter λ depends on the flow regime and the properties of the materials.

The distribution of stresses is governed by[56]

$$-\frac{\partial\tilde{\sigma}_x}{\partial\tilde{x}} - \frac{\partial\tilde{\tau}_{xy}}{\partial\tilde{y}} - \frac{\partial\tilde{\tau}_{xz}}{\partial\tilde{z}} = 0, \quad (12)$$

$$-\frac{\partial\tilde{\tau}_{xy}}{\partial\tilde{x}} - \frac{\partial\tilde{\sigma}_y}{\partial\tilde{y}} - \frac{\partial\tilde{\tau}_{yz}}{\partial\tilde{z}} = 0, \quad (13)$$

$$-\frac{\partial\tilde{\tau}_{xz}}{\partial\tilde{x}} - \frac{\partial\tilde{\tau}_{yz}}{\partial\tilde{y}} - \frac{\partial\tilde{\sigma}_z}{\partial\tilde{z}} = 0, \quad (14)$$

and the stress-strain relationship for an isotropic material

$$\begin{bmatrix} \varepsilon_x \\ \varepsilon_y \\ \varepsilon_z \\ \gamma_{xy} \\ \gamma_{yz} \\ \gamma_{xz} \end{bmatrix} = \frac{1}{\tilde{E}} \begin{bmatrix} 1 & -\nu & -\nu & 0 & 0 & 0 \\ -\nu & 1 & -\nu & 0 & 0 & 0 \\ -\nu & -\nu & 1 & 0 & 0 & 0 \\ 0 & 0 & 0 & 2(1+\nu) & 0 & 0 \\ 0 & 0 & 0 & 0 & 2(1+\nu) & 0 \\ 0 & 0 & 0 & 0 & 0 & 2(1+\nu) \end{bmatrix} \begin{bmatrix} \tilde{\sigma}_x \\ \tilde{\sigma}_y \\ \tilde{\sigma}_z \\ \tilde{\tau}_{xy} \\ \tilde{\tau}_{yz} \\ \tilde{\tau}_{xz} \end{bmatrix}, \quad (15)$$

where ε is the normal strain, γ is the shear strain, and ν is the Poisson ratio. The strain-displacement relationships for small displacements are

$$\varepsilon_x = \frac{\partial\tilde{u}}{\partial\tilde{x}}, \quad \varepsilon_y = \frac{\partial\tilde{v}}{\partial\tilde{y}}, \quad \varepsilon_y = \frac{\partial\tilde{w}}{\partial\tilde{z}}, \quad (16)$$

$$\gamma_{xy} = \frac{\partial\tilde{u}}{\partial\tilde{y}} + \frac{\partial\tilde{v}}{\partial\tilde{x}}, \quad \gamma_{yz} = \frac{\partial\tilde{v}}{\partial\tilde{z}} + \frac{\partial\tilde{w}}{\partial\tilde{y}}, \quad \gamma_{xz} = \frac{\partial\tilde{u}}{\partial\tilde{z}} + \frac{\partial\tilde{w}}{\partial\tilde{x}}. \quad (17)$$

The damping effect is assumed negligible. The von Mises stress is used as the yield criterion

$$\tilde{\sigma}_{vM} = 2^{-1/2}\left[(\tilde{\sigma}_x - \tilde{\sigma}_y)^2 + (\tilde{\sigma}_y - \tilde{\sigma}_z)^2 + (\tilde{\sigma}_z - \tilde{\sigma}_x)^2\right]^{1/2}. \quad (18)$$

The dimensionless thermal strain depends on the present temperature, θ, the stress-free reference temperature, θ_{ref}, and the thermal expansion vector, $\tilde{\alpha}_{vec}$,

$$\varepsilon_{th} = \begin{bmatrix} \varepsilon_x \\ \varepsilon_y \\ \varepsilon_z \\ \gamma_{xy} \\ \gamma_{yz} \\ \gamma_{xz} \end{bmatrix} = \tilde{\alpha}_{vec}(\theta - \theta_{ref}). \quad (19)$$

The vector $\tilde{\alpha}_{vec}$ for an isotropic material is

$$\tilde{\alpha}_{vec} = \begin{bmatrix} \tilde{\alpha} \\ \tilde{\alpha} \\ \tilde{\alpha} \\ 0 \\ 0 \\ 0 \end{bmatrix}, \quad (20)$$

where $\tilde{\alpha} = \alpha(q''L/k_s)$. The boundary conditions for stresses are as follows. The surfaces on the plane $\tilde{x} = 1$ are fixed. The remaining surfaces are free. The downward pressure $\tilde{P}_{mech} = 1$ is applied uniformly on the top surface. In addition, we assumed $\phi = 0.05$, $\tilde{E} = 2 \times 10^5$, $\tilde{\alpha} = 2 \times 10^{-5}$, $\nu = 0.33$, and $\tilde{k}_s = 1$, where the dimensionless definition of the thermal conductivity is given by $\tilde{k} = k/k_s$.

The computations were performed in dimensionless form by using a finite element package.[57] In order to confirm whether or not the solution is independent from the size of mesh, the solution was first performed with a coarse mesh, and then it was performed again using finer meshes until the changes in the maximum temperature and the maximum von Mises stress become of order of 2%. Figure 3(a) shows the temperature distribution when the angle $\alpha = 25°$ and the parameter $\lambda = 10$. The maximum temperatures, θ_{max}, or peak temperatures are distributed in both sides of the cooling channel located in the upper surface of the slab. Figure 3(b) shows the von Mises stress distribution. The highest von Mises stress, $\sigma_{vM,max}$, is located approximately in the corner (1, 0, 0.1). This stress is approximately 100% higher than the von Mises lower stress shown in the corner (1, 1, 0.1).

Figure 4(a) shows the behavior of θ_{max} and $\sigma_{vM,max}$ as a function of α. The parameter λ is fixed $\lambda = 10$. The results indicate that there is a pronounced minimal θ_{max} when $\alpha_{opt} \approx 26°$. This value is approximately 30% smaller than the value of θ_{max} when $\alpha = 10°$ and 20% smaller than the value of θ_{max} when $\alpha = 40°$. This figure also shows that $\sigma_{vM,max}$ presents a minimum as the angle $\alpha_{opt} = 23°$. This value is approximately 55% smaller than the highest $\sigma_{vM,max}$ calculated for the extremes $\alpha = 5°$ and $\alpha = 40°$. In Fig. 4(b), θ_{max} is represented on the abscissas and $\sigma_{vM,max}$ on the ordinate. The corresponding values are plotted for several values of the angle α. Smaller θ_{max} and $\sigma_{vM,max}$ are obtained when the points are closer to the bottom-left corner. This figure shows that smaller θ_{max} and $\sigma_{vM,max}$ are achievable in the range $23° \leq \alpha \leq 27°$.

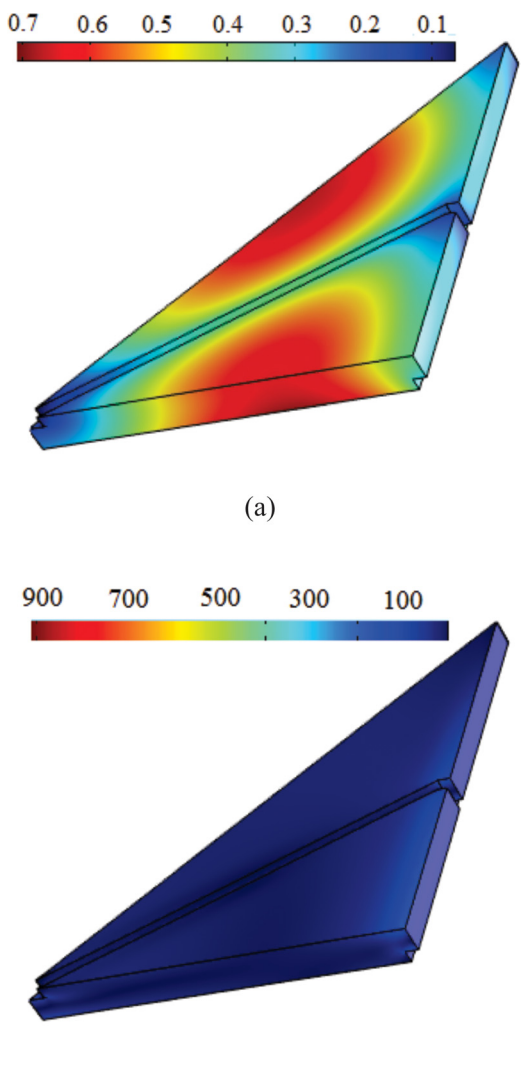

FIG. 3. The temperature distribution (a) and von Mises stress distribution when the angle $\beta = 25°$ and the parameter $\lambda = 10$.

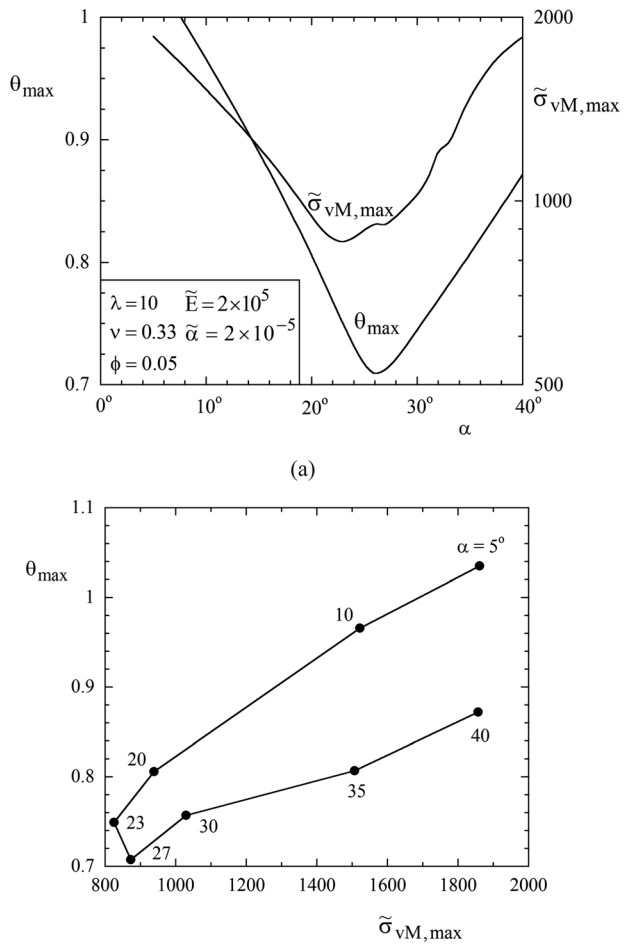

FIG. 4. The effect of the β angle on the maximum temperature and the maximum von Mises stress when $\lambda = 10$.

Figure 5(a) shows the behavior of θ_{max} and $\sigma_{vM,max}$ as functions of the angle α when $\lambda = 1$. There is a shallow minimum in the θ_{max} curve in the vicinity of $\alpha = 25°$. The minimum θ_{max} is 13% smaller than the θ_{max} value when $\alpha = 5°$, but only 1% smaller than θ_{max} at $\alpha = 40°$. The $\sigma_{vM,max}$ exhibits a pronounced minimum when $\alpha = 23°$. Figure 5(b) indicates that the angle $\alpha = 27°$ is recommended when the goal is to select a configuration with smaller maximum temperature and von Mises stress. Figure 6(a) shows the behavior of θ_{max} and $\sigma_{vM,max}$ as a function of the angle α when $\lambda = 0.5$. Now the maximum temperature decreases monotonically when α increases, and it reaches its smallest θ_{max} value at $\alpha = 40°$. The $\sigma_{vM,max}$ curve has a sharp minimum when $\alpha = 23°$. The summary presented in Fig. 6(b) indicates that $\alpha \cong 27°$ is again the winning design.

The maximum temperature as a function of α is presented in Fig. 7(a) for several values of the parameter λ. The minimum θ_{max} decreases as λ increases and it reaches its minimal value $\theta_{max} = 0.366$ when $\alpha_{opt} = 26°$ and $\lambda = \infty$, i.e., when the fluid-solid interface is isothermal. The θ_{max} minimum becomes less pronounced as λ decreases; its corresponding optimal α increases as λ decreases and reaches $\alpha_{opt} = 40°$ when $\lambda = 0.5$. Figure 7(b) summarizes the $\sigma_{vM,max}$ results as function of α and λ. The maximum von Mises stress decreases as λ increases, indicating that $\alpha_{opt} = 23°$.

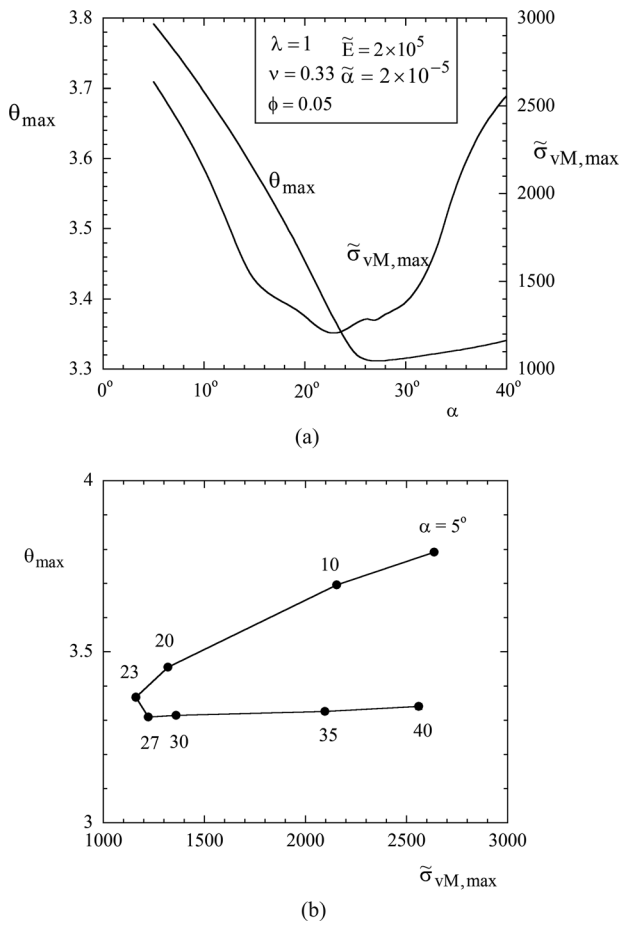

FIG. 5. The effect of the β angle on the maximum temperature and the maximum von Mises stress when $\lambda = 1$.

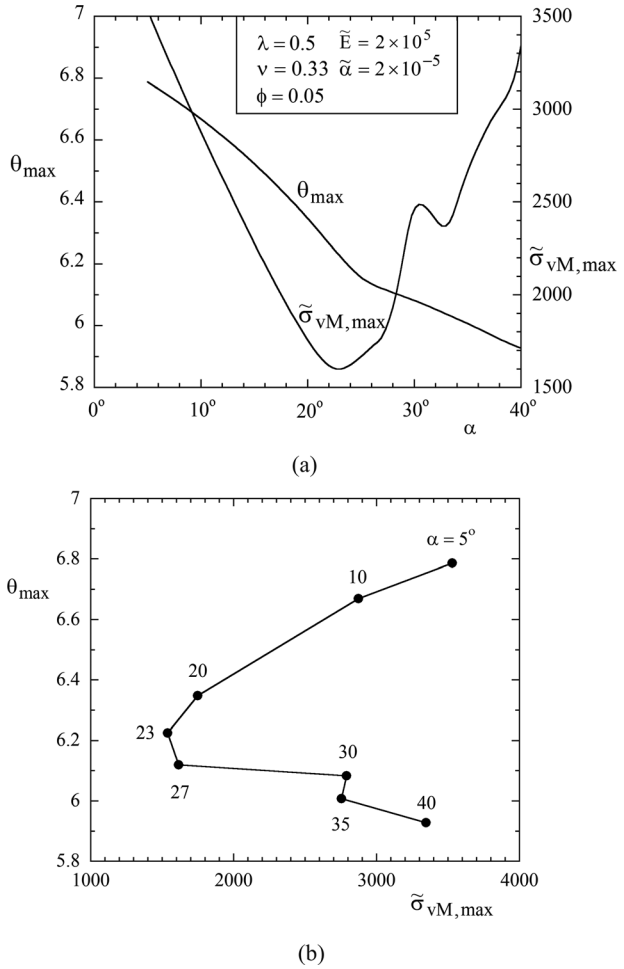

FIG. 6. The effect of the β angle on the maximum temperature and the maximum von Mises stress when $\lambda = 0.5$.

We repeated the simulations presented in Figs. 4–6 for several values of the parameter λ, and collected the minimum θ_{max} and $\sigma_{vM,max}$ values, which are labeled $\theta_{max,min}$ and $\sigma_{vM,max,min}$ in Fig. 8. Notice that $\theta_{max,min}$ decreases as λ increases; its corresponding optimal angle $\alpha_{opt} = 26°$ is constant except for $\lambda < 0.8$, when it decreases almost abruptly to $\alpha_{opt} = 40°$. Figure 8(b) shows that $\sigma_{vM,max,min}$ also decrease as λ increases, and reaches its lowest value when $\lambda > 100$. If the objective is small von Mises stress only, the recommended value is $\alpha_{opt} = 23°$ for the entire range of the parameter λ.

III. DENDRITIC DESIGN WITH ONE LEVEL BIFURCATION

Consider next the design with Y-shaped channels shown in Fig. 9. The structure is similar to Fig. 2, except that the duct bifurcates into two branches that form the angle β. The volume occupied by the ducts is

$$V_p = V_a + V_b + V_c + V_d + V_e, \qquad (21)$$

where

$$V_a = \left(\frac{\sin(\pi/4 + \alpha)\sin(\pi/2 - \alpha)}{2\sin(\pi/4)} D_0 + L_0\right) D_0^2, \qquad (22)$$

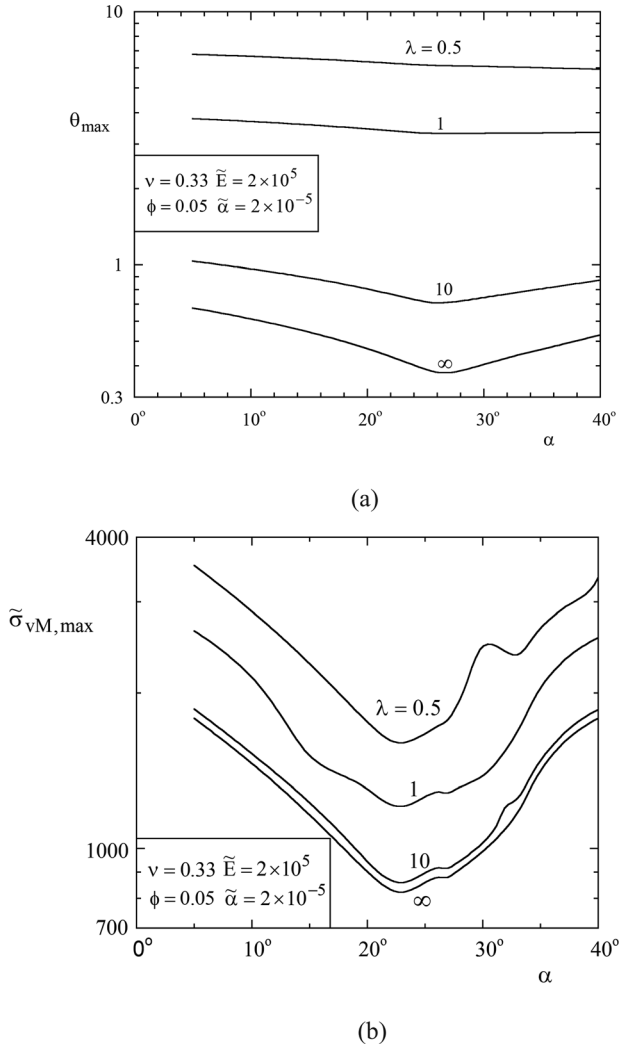

FIG. 7. The effect of the angle β and the parameter λ on the maximum temperature and maximum von Mises stress.

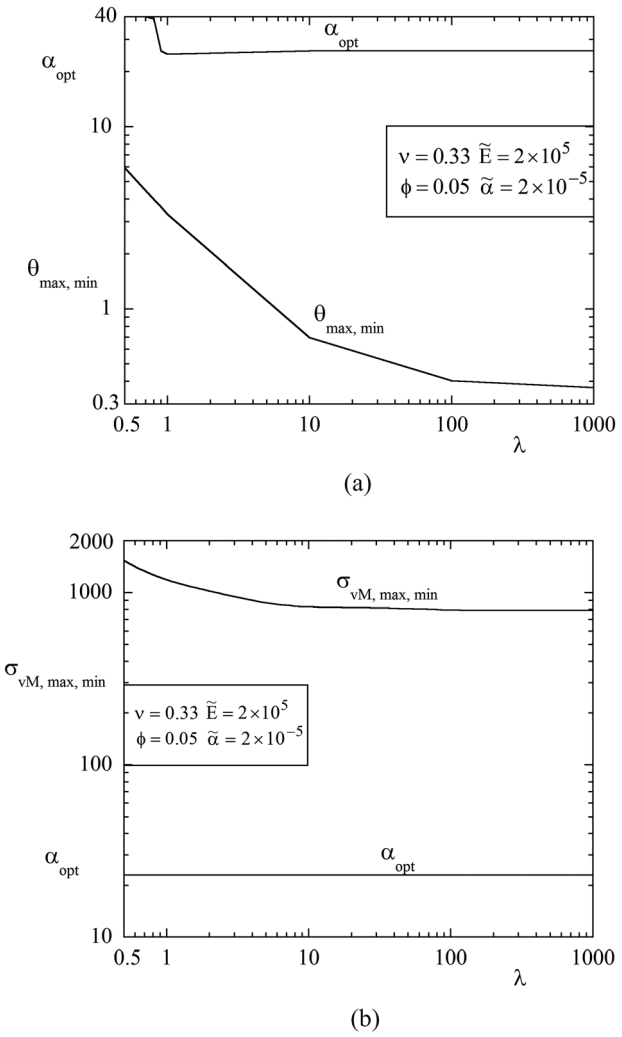

FIG. 8. The effect of the parameter λ on the minimal maximal temperature, minimal maximal von Mises stress, and optimal angle α.

$$V_b = (L_1 + t)D_1^2, \tag{23}$$

$$V_c = (L_2 + t)D_2^2, \tag{24}$$

$$V_d = y_1 D_1^2 + hD_2^2 + (L - y_1 - h - 2D_1 - D_2)D_2^2, \tag{25}$$

$$V_e = \frac{1}{2}D_1^3, \tag{26}$$

and where the dimension h should not be confused with the heat transfer coefficient employed in Eq. (10). The resulting structure has more degrees of freedom than in Fig. 2. To begin with, the channel size ratios D_0/D_1 and D_0/D_2 vary, but their optimal values are not the same as those recommended by the Hess-Murray rule ($D_0/D_1 = D_0/D_2 = 2^{1/3}$). It was shown that the Hess-Murray rule is valid only when the Y-shaped construct has two identical branches ($L_1 = L_2$, $D_1 = D_2$), and that in general, the optimized D ratios depend on the L ratios as follows:[27]

$$\frac{D_0}{D_1} = \left[1 + \left(\frac{L_2}{L_1}\right)^3\right]^{1/3}, \tag{27}$$

$$\frac{D_0}{D_2} = \left[1 + \left(\frac{L_1}{L_2}\right)^3\right]^{1/3}. \tag{28}$$

Because of Eqs. (27) and (28), the design of Fig. 9 has four degrees of freedom, namely y_1, h, L_0, and α.

We optimized the dendritic design of Fig. 9 in the same way as the radial design of Fig. 2. We searched for the configuration with minimum θ_{max} and $\sigma_{vM,max}$ regardless of their locations. Figure 10 illustrates the distribution of temperature and von Mises stress when $\alpha = 30°$, $\tilde{L}_0 = 0.6$, $\tilde{y}_1 = 0.24$, $\tilde{h} = 0.18$, and $\lambda = 10$. Figure 11(a) shows the behavior of θ_{max} and $\sigma_{vM,max}$ as functions of α. The parameter λ is fixed $\lambda = 10$, and the other degrees of freedom are $\tilde{L}_0 = 0.6$, $\tilde{y}_1 = 0.24$, $\tilde{h} = 0.18$. This figure indicates that θ_{max} and $\sigma_{vM,max}$ exhibit their minima at the same angle, $\alpha = 22°$, i.e., one design reduces both the hot spots and the thermal stresses. These results are also presented in Fig. 11(b) to emphasize the behavior discovered in Fig. 11(a). Later, we kept $\lambda = 10$, $\tilde{y}_1 = 0.24$, and $\tilde{h} = 0.18$, and repeated the procedure of Figure 11, by varying $\tilde{L}_0$ for several angles α. Figure 12 shows that in general θ_{max} and $\sigma_{vM,max}$ decrease as

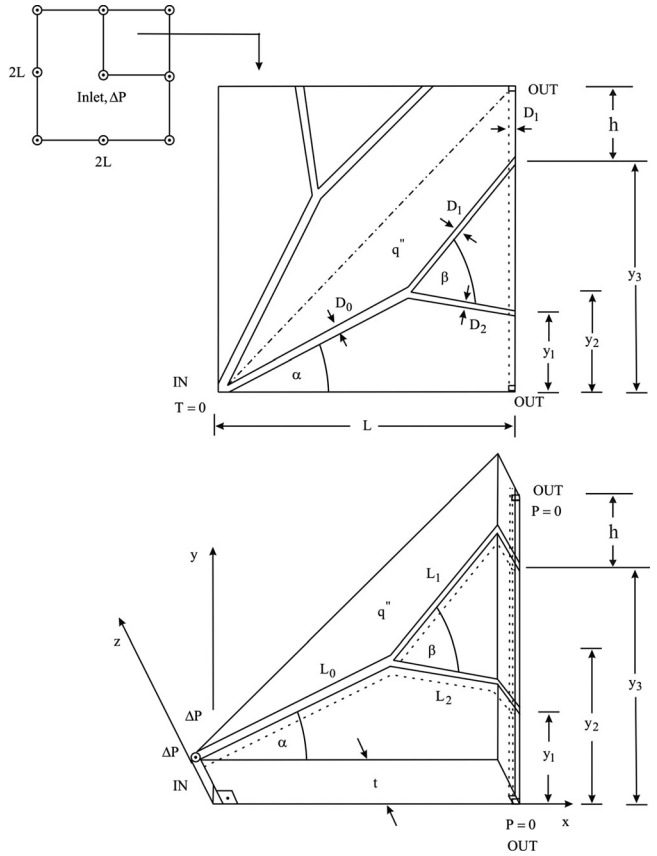

FIG. 9. Configuration design with one level of bifurcation.

$\tilde{L}_0$ and α decrease, and that θ_{max} and $\sigma_{vM,max}$ reach their minimum values in the range $18^\circ \leq \alpha \leq 22^\circ$ depending on the value of $\tilde{L}_0$. However, after the minimum value for $\sigma_{vM,max}$

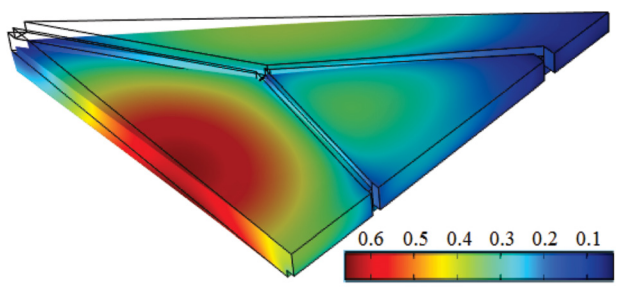

(a)

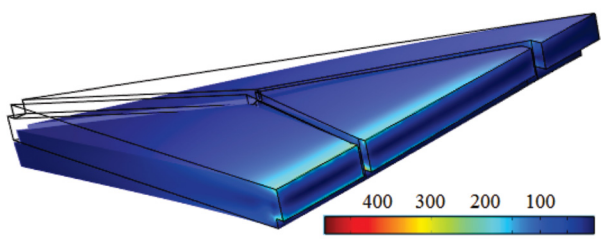

(b)

FIG. 10. Temperature distribution and von Mises stress distribution in the configuration with one level of bifurcation when $\alpha = 30^\circ$ and $\lambda = 10$.

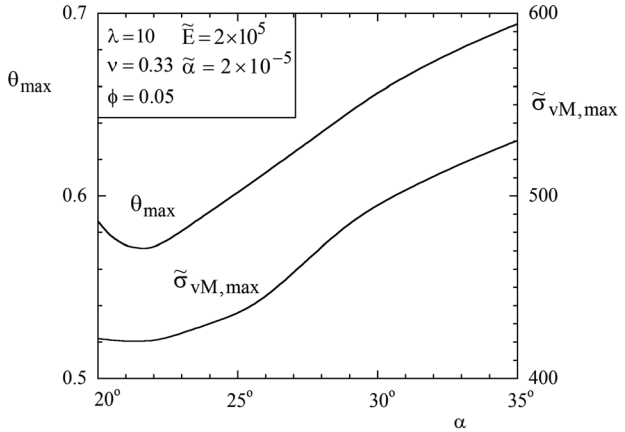

(a)

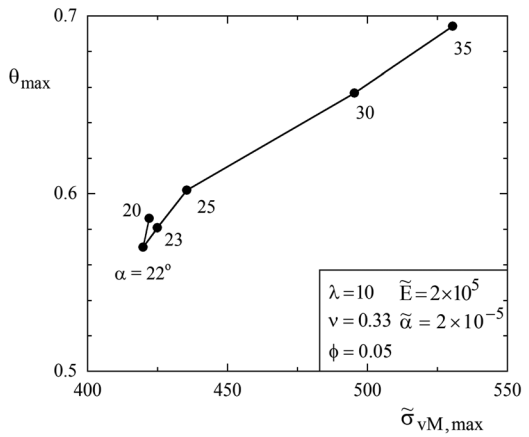

(b)

FIG. 11. Configuration with one level of bifurcation: the effect of the angle α on the maximum temperature and the maximum von Mises stress when $\lambda = 10$.

is reached when $\tilde{L}_0 = 0.36$, the pattern changes such that diminishing the value of $\tilde{L}_0$ does not decrease the stress. This is why the configuration with $\tilde{L}_0 = 0.36$ and $\alpha = 18^\circ$ is the best configuration. For example, the configuration with

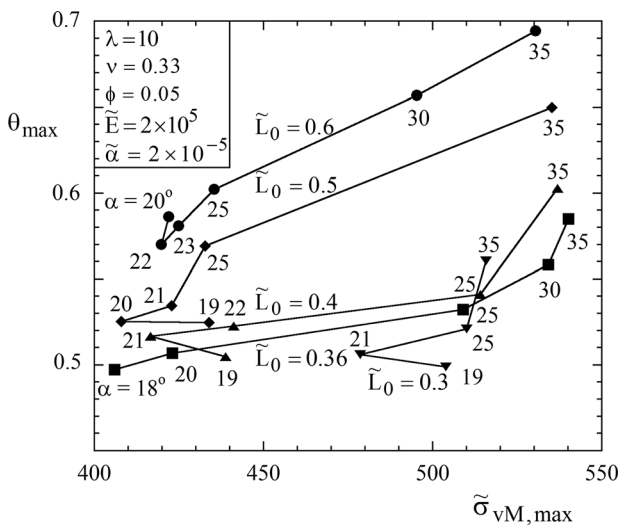

FIG. 12. Design with one level of bifurcation: the effect of the length $\tilde{L}_0$ and the angle α on the maximum temperature and von Mises stress when $\lambda = 10$.

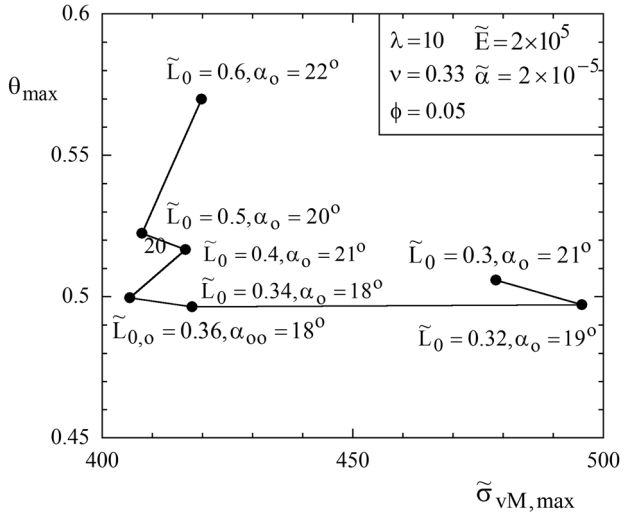

FIG. 13. Summary of the configurations with the optimal angle α_o calculated for each length $\tilde{L}_0$ in Fig. 12.

the curve for $\tilde{L}_0 = 0.3$ and $\alpha = 19°$ has a similar thermal performance when compared with $\tilde{L}_0 = 0.36$ and $\alpha = 18°$, but its value of $\sigma_{vM,max}$ is much larger than the one obtained for the design with $\tilde{L}_0 = 0.36$ and $\alpha = 18°$.

The results presented in Fig. 12 are summarized in Fig. 13, where the configurations with the optimal angle α_o calculated for each length $\tilde{L}_0$ are shown. Close examination of Fig. 13 confirms the configuration with the optimal length $\tilde{L}_{0,o} = 0.36$ and the twice optimized angle $\alpha_{oo} = 18°$ as the configuration that reduces simultaneously the hot spots and the von Mises stresses the most. When compared to the radial configuration in the same thermal conditions (Fig. 4), this configuration reduces approximately 28% the hot spots and 53% the peak stresses. It is important to notice that the optimal α angle calculated for the one level of bifurcation ($\alpha_o = 18°$) is smaller than the optimal range calculated for the radial configuration ($23° \leq \alpha \leq 27°$).

IV. CONCLUDING REMARKS

In this paper, we developed the design of a vascular flow structure for plate subjected to heating and mechanical loading. We showed how to determine the flow architecture that offers minimum peak temperatures and peak stresses. The flow architecture is configured as a patchwork of elemental square-shaped slabs, each cooled with a tree-shaped vasculature (Fig. 1). The coolant enters through the center of the element and exits through ports distributed along the square perimeter.

The numerical simulations of heat flow and thermal stresses in three dimensions showed that it is possible to optimize the main features of the tree-shaped configuration. As the complexity of each tree increases from radial channels to one level of bifurcation, the global thermal resistance and the peak stresses of the architecture decrease for the considered thermal condition.

In future work, the methodology developed in this paper can be extended to situations where the mechanical load and the heating load are oriented in the same direction. In the present work, the mechanical and heating loads were oriented in opposite directions. The study of the effect of the two remaining degrees of freedom, $\tilde{y}_1$ and $\tilde{h}$, in the configuration with one level of bifurcation can lead to configurations with better performance. Later, configurations with two or three level of bifurcations can also be investigated.

ACKNOWLEDGMENTS

Professor Bejan and Professor Lorente's research was supported by the National Science Foundation. Professor Rocha's research was supported by CNPq, Brasília, DF, Brazil.

[1]A. Bejan, "Constructal-theory network of conducting paths for cooling a heat generating volume," Int. J. Heat Mass Transfer **40**, 799–816 (1997) (cf. Fig. 3).
[2]A. Bejan, *Advanced Engineering Thermodynamics*, 2nd ed. (Wiley, New York, 1997).
[3]G. A. Ledezma, A. Bejan, and M. Errera, "Constructal tree networks for heat transfer," J. Appl. Phys. **82**, 89–100 (1997).
[4]M. R. Errera and A. Bejan, "Deterministic tree networks for river drainage basins," Fractals **6**, 245–261 (1998).
[5]A. Bejan, *Shape and Structure from Engineering to Nature* (Cambridge University Press, Cambridge, UK, 2000).
[6]A. Bejan and S. Lorente, "Constructal law of design and evolution: Physics, biology, technology, and society," J. Appl. Phys. **113**, 151301 (2013).
[7]T. Basak, "The law of life: The bridge between physics and biology," Phys. Life Rev. **8**, 249–252 (2011).
[8]A. Bejan and S. Lorente, "Constructal theory of generation of configuration in nature and engineering," J. Appl. Phys. **100**, 041301 (2006).
[9]A. Bejan and J. P. Zane, *Design in Nature: How the Constructal Law Governs Evolution in Biology, Physics, Technology, and Social Organization* (Doubleday, New York, 2012).
[10]A. H. Reis, "Constructal theory: From engineering to physics, and how flow systems develop shape and structure," Appl. Mech. Rev. **59**, 269–282 (2006).
[11]A. Bejan and S. Lorente, "The constructal law of design and evolution in nature," Phil. Trans. R Soc. B **365**, 1335–1347 (2010).
[12]L. Chen, "Progress in study on constructal theory and its applications," Sci. China: Technol. Sci. **55**(3), 802–820 (2012).
[13]A. Bejan, S. Lorente, and K.-M. Wang, "Networks of channels for self-healing composite materials," J. Appl. Phys. **100**, 033528 (2006).
[14]K.-M. Wang, S. Lorente, and A. Bejan, "Vascularized networks with two optimized channels sizes," J. Phys. D: Appl. Phys. **39**, 3086–3096 (2006).
[15]S. Kim, S. Lorente, and A. Bejan, "Vascularized materials: Tree-shaped flow architectures matched canopy to canopy," J. Appl. Phys. **100**, 063525 (2006).
[16]J. Lee, S. Lorente, and A. Bejan, "Vascular design for thermal management of heated structures," Aeronaut. J. **113**, 397–407 (2009).
[17]A. Bejan and M. R. Errera, "Convective trees of fluid channels for volumetric cooling," Int. J. Heat Mass Transfer **43**, 3105–3118 (2000).
[18]S. Kim, S. Lorente, A. Bejan, W. Miller, and J. Morse, "The emergence of vascular design in three dimensions," J. Appl. Phys. **103**, 123511 (2008).
[19]E. Cetkin, S. Lorente, and A. Bejan, "Natural constructal emergence of vascular design with turbulent flow," J. Appl. Phys. **107**, 114901 (2010).
[20]A. M. Aragón, R. Saksena, B. D. Kozola, P. H. Geubelle, K. T. Cristensen, and S. R. White, "Multi-physics optimization of three-dimensional microvascular polymeric components," J. Comput. Phys. **233**, 132–147 (2013).
[21]S. Soghrati, P. R. Thakre, S. R. White, N. R. Sottos, and P. H. Geubelle, "Computational modeling and design of actively-cooled microvascular materials," Int. J. Heat Mass Transfer **55**, 5309–5321 (2012).
[22]K.-H. Cho, W.-P. Chang, and M.-H. Kim, "A numerical and experimental study to evaluate performance of vascularized cooling plates," Int. J. Heat Fluid Flow **32**, 1186–1198 (2011).
[23]K.-H. Cho and C.-W. Choi, "Hydraulic-thermal performance of vascularized cooling plates with semi-circular cross-section," Appl. Therm. Eng. **33–34**, 157–166 (2012).

[24]W. Wechsatol, J. C. Ordonez, and S. Kosaraju, "Constructal dendritic geometry and the existence of asymmetric bifurcation," J. Appl. Phys. **100**, 113514 (2006).
[25]M. S. Sayeed, I. A. Ahmed, A. A. Syed, P. H. Raju, and M. S. Salman, "Experimental study of tree networks for minimal pumping power," Int. J. Des. Nat. Ecodyn. **3**, 135–149 (2008).
[26]R. Godde and H. Kurz, "Structural and biophysical simulation of angiogenesis and vascular remodeling," Dev. Dyn. **220**, 387–401 (2001).
[27]L. Gosselin, "Optimization of tree-shaped fluid networks with size limitations," Int. J. Therm. Sci. **46**, 434–443 (2007).
[28]Y. Kwak, D. Pence, J. Liburdy, and V. Narayanan, "Gas-liquid flows in a microscale fractal-like branching flow networks," Int. J. Heat Fluid Flow **30**, 868–876 (2009).
[29]K.-H. Cho and M.-H. Kim, "Transient thermal-fluid flow characteristics of vascular networks," Int. J. Heat Mass Transfer **55**, 3533–3540 (2012).
[30]A. M. Aragón, J. K. Wayer, P. H. Geubelle, D. E. Goldberg, and S. R. White, "Design of microvascular flow networks using multi-objective genetic algorithms," Comput. Methods Appl. Mech. Eng. **197**, 4399–4410 (2008).
[31]K.-H. Cho and M.-H. Kim, "Fluid flow characteristics of vascularized channel networks," Chem. Eng. Sci. **65**, 6270–6281 (2010).
[32]R. Boichot and L. Luo, "A simple cellular automaton algorithm to optimise heat transfer in complex configurations," Int. J. Exergy **7**, 51–64 (2010).
[33]X.-Q. Wang, P. Xu, A. S. Mujumdar, and C. Yap, "Flow and thermal characteristics of offset branching network," Int. J. Therm. Sci. **49**, 272–280 (2010).
[34]T. Bello-Ochende, J. P. Meyer, and F. U. Ighalo, "Combined numerical optimization and constructal theory for the design of microchannel heat sinks," Numer. Heat Transfer Part A **58**, 882–899 (2010).
[35]Y. Chen, C. Zhang, M. Shi, and Y. Yang, "Thermal and hydrodynamic characteristics of constructal tree-shaped minichannel heat sink," AIChE J. **56**, 2018–2029 (2009).
[36]Y. S. Muzychka, "Constructal multi-scale design of compact micro-tube heat sinks and heat exchangers," Int. J. Therm. Sci. **46**, 245–252 (2007).
[37]Y. S. Muzychka, "Constructal design of forced convection cooled microchannel heat sinks and heat exchangers," Int. J. Heat Mass Transfer **48**, 3119–3127 (2005).
[38]M. R. Salimpour, M. Sharifhasan, and E. Shirani, "Constructal optimization of the geometry of an array of micro-channels," Int. Comm. Heat Mass Transfer **38**, 93–99 (2011).
[39]D. Haller, P. Woias, and N. Kockmann, "Simulation and experimental investigation of pressure loss and heat transfer in microchannel networks containing bends and T-junctions," Int. J. Heat Mass Transfer **52**, 2678–2689 (2009).
[40]S. Lorente, "Constructal view of electrokinetic transfer through porous media," J. Phys. D: Appl. Phys. **40**, 2941–2947 (2007).
[41]X. Zeng, W. Dai, and A. Bejan, "Vascular countercurrent network for 3-D triple-layered skin structure with radiation heating," Numer. Heat Transfer A **57**, 369–391 (2010).
[42]X. Tang, W. Dai, R. Nassar, and A. Bejan, "Optimal temperature distribution in a three-dimensional triple-layered skin structure embedded with artery and vein vasculature," Num. Heat Transfer A **50**, 809–834 (2006).
[43]K.-C. Liu, Y.-N. Wang, and Y.-S. Chen, "Investigation on the bio-heat transfer with dual-phase-lag effect," Int. J. Therm. Sci. **58**, 29–35 (2012).
[44]P. Yuan, S.-B. Wang, and H.-M. Lee, "Estimation of the equivalent perfusion rate of Pennes model in an experimental bionic tissue without blood flow," Int. Comm. Heat Mass Transfer **39**, 236–241 (2012).
[45]E. Cetkin, S. Lorente, and A. Bejan, "Vascularization for cooling a plate heated by a randomly moving source," J. Appl. Phys. **112**, 084906 (2012).
[46]A. Bejan, "The constructal-law origin of the wheel, size, and skeleton in animal design," Am. J. Phys. **78**, 692–699 (2010).
[47]A. Bejan, S. Lorente, and J. Lee, "Unifying constructal theory of tree roots, canopies and forests," J. Theor. Biol. **254**, 529–540 (2008).
[48]S. Lorente and A. Bejan, "Few large and many small: Hierarchy in movement on earth," Int. Des. Nat. Ecodyn. **5**, 254–267 (2010).
[49]A. Bejan and S. Lorente, *Design with Constructal Theory* (Wiley, Hoboken, 2008).
[50]S. Lorente, J. Lee, and A. Bejan, "The flow of stresses concept: The analogy between mechanical strength and heat convection," Int. Heat Mass Trans. **53**, 2963–2968 (2010).
[51]E. Cetkin, S. Lorente, and A. Bejan, "Vascularization for cooling and mechanical strength," Int. J. Heat Mass Trans. **54**, 2774–2781 (2011).
[52]E. Cetkin, S. Lorente, and A. Bejan, "Hybrid grid and tree structures for cooling and mechanical strength," J. Appl. Phys. **110**, 064910 (2011).
[53]L. Chen, Z. Xie, and F. Sun, "Multiobjective constructal optimization of an insulating wall combining heat flow, strength, and weight," Int. J. Thermal Sci. **50**, 1782–1789 (2011).
[54]A. Bejan, *Convection Heat Transfer*, 3rd ed. (Wiley, New York, 2004).
[55]L. A. O. Rocha, S. Lorente, and A. Bejan, "Tree-shaped vascular wall designs for localized intense cooling," Int. J. Heat Mass Transfer **52**, 4535–4544 (2009).
[56]K.-M. Wang, S. Lorente, and A. Bejan, "Vascular structures for volumetric cooling and mechanical strength," J. Appl. Phys. **107**, 044901 (2010).
[57]See www.comsol.com to consult the user manual.